Water Utility Journal 29: 29-42, 2021.

On the numerical modeling of non-hydrostatic flows with dual free surfaces

Y. T. Zerihun*

David & James - Engineering and Environmental Consultancy, 204 Albion Road, Victoria 3350, Australia
* *e-mail: zyebegaeshet@gmail.com*

Abstract: The free overfall can be used as a metering device for discharge in open channels. In earlier works, the solutions to the free-overfall problem were generally found on the basis of empirical relations stemming from measurements or through the application of a simplified theoretical method. For this type of curved-flow problem, the hydrostatic pressure approach is no longer valid. In this study, the Boussinesq approach for treating the effects of the vertical acceleration, along with the assumption of a linear variation of horizontal velocity across the flow depth, is employed to develop a non-hydrostatic numerical model. The suitability of the proposed model is investigated by simulating curvilinear overfalls in rectangular channels with smooth and rough beds. The computed results for velocity distribution at different sections and free-surface and pressure profiles were systematically compared with the experimental data, thereby resulting in a remarkable agreement. Overall, the results of this study exhibited the validity of the model in simulating complex transition between subcritical and supercritical flow regimes and hence highlighted the potential of the current computational scheme for developing a discharge rating curve for free overfall with a subcritical approach flow.

Key words: Free overfall; finite-difference method; flow measurement; hydraulic structure; rapidly-varied flow; non-hydrostatic flow

1. INTRODUCTION

In the past, the dynamics of free-surface flows have been the subject of many experimental and theoretical studies. For a regulated streamflow, the outcomes of such studies have been used for developing an effective water management plan and operating rules. In a regulated open-channel flow system, a hydraulic structure such as a drop structure may be used as a metering device for discharge (Bos, 1989, p. 326). One of the main flow features of a drop structure is the free overfall, which is characterized by a departure from the hydrostatic pressure distribution caused by the strong vertical curvatures of the streamline in the vicinity of the drop brink. For this type of flow situation, the depth-averaged Saint-Venant equations, which rely on an important assumption of negligible vertical acceleration, are no longer valid. For the free-overfall problem, the effect of the dynamic pressure needs to be properly accounted for so as to develop a depth-averaged model which is capable of describing the two-dimensional (2D) structure of the flow field. From a practical perspective, such a type of numerical model can effectively supplement expensive physical model tests, especially for establishing the brink-depth-discharge relationships for free overfall with a subcritical approach flow.

The problem of a laterally-guided free overfall as a discharge measuring device has been extensively studied experimentally, analytically, and numerically. Rouse (1932, 1933), Rajaratnam and Muralidhar (1968), and Rajaratnam et al. (1976) were carried out detailed experimental analyses to investigate the flow characteristics of a rectangular free overfall, including the distributions of velocity and pressure. Besides, several theoretical and experimental investigations have been conducted to understand the hydraulics of the end-depth (brink-depth) problem and to determine the end-depth ratio in channels with various cross-sectional shapes. A comprehensive

review of these investigations was presented by Dey (2002).

Solutions of the potential-flow theory to determine the hydraulic characteristics of the free overfall in a rectangular channel were given by Jaeger (1948), Montes (1992), Marchi (1993), and Guo (2005). Even though the assumption of irrotational flow is reasonable for converging flow situations (see, e.g., Le Méhauté, 1969, p. 354), this approach cannot take into account the effects of turbulence. A higher-order energy form of an open-channel flow equation, which considers the rotational effect of the curvilinear flow, was developed and applied by Nakagawa (1969) to analyze the internal structure of the free overfall. Khan (1999) also applied the Boussinesq-type equations to solve the rectangular free-overfall problem numerically. The equations were developed by depth-averaging the 2D Reynolds-averaged Navier-Stokes (RANS) equations based on the assumptions of a linear variation of vertical velocity and non-hydrostatic pressure distributions. However, the numerical solution of the pressure equation is unrealistic, especially for the free jet portion of the flow close to the brink section, where the pressure at the free surfaces of the nappe is atmospheric. Results of the pressure distribution measurements by Rouse (1932) and Rajaratnam and Muralidhar (1968) demonstrate that the internal pressure is non-atmospheric in this flow region due to the converging nature of the streamlines. Likewise, Ramamurthy et al. (2005, 2006) and Guo et al. (2008) applied the volume of fluid method based on the RANS equations to arrive at the solutions of the free-overfall problem. In addition, machine learning techniques (Raikar et al., 2004; Pal and Goel, 2006, 2007; Sharifi et al., 2010), an approach based on the RANS equations with a weakly-curved flow approximation (Bose and Dey, 2007), and the energy principle along with the Boussinesq approximation for analyzing the solitary wave (Di Nucci and Russo Spena, 2018) were employed to model the local flow characteristics of the free overfall in open channels. Despite the aforementioned extensive investigation of the free-overfall problem, little effort has been made to develop a general-purpose model which is capable of simulating the 2D flow structure by treating the fixed bed and the free jet portion of the flow as a single curved-flow problem. Some of the existing higher-order numerical methods (e.g., Castro-Orgaz and Hager, 2011), which consider only the fixed bed part of the flow, lacked terms that account for the effects of the curvature of the lower nappe at the brink section. Hence, the results of such methods, especially for the local flow characteristics at this section, are questionable. As a remedial measure for improving the accuracy of the methods, an approximate procedure based on the slope and curvature of a parabolic lower nappe profile was introduced by Jaeger (1948), Marchi (1993), and Matthew (1995).

Recently, Fenton and Zerihun (2007) developed a Boussinesq-type momentum model based on the assumption of a constant horizontal velocity across a vertical section. Their model gave reliable solutions to the curvilinear flow problems, especially for the global flow characteristics. For a better recovery of the necessary flow details over the vertical dimension, this model was extended without resorting to the lowest-order approximation for the vertical profiles of the horizontal velocity and streamline geometry parameter (Zerihun, 2021). Such a depth-averaged model incorporates a higher-order correction for the effects of the vertical curvatures of the streamline, thereby accurately describing the rapidly-varied flow situations. Therefore, the main objectives of this study are to: (i) investigate the feasibility of this Boussinesq-type model for a more complicated steady-flow problem involving dual free surfaces such as a rectangular free overfall; (ii) examine the effect of the vertical curvatures of the streamline on the solutions of the model; and (iii) demonstrate the validity of the results of the model by a number of existing experimental data for sub- and super-critical inflow conditions.

Following a brief summary of the derivation of the governing equations, the paper describes the spatial discretization of the equations using the finite-difference method. The solution procedures for the resulting non-linear discretized equations are also outlined with reference to the case study. In Section 3, a brief discussion of the comparison of the numerical results with the experimental data is presented. Finally, the paper ends with a discussion and conclusions.

2. NUMERICAL METHODOLOGY

2.1 Governing equations

The longitudinal profile of a rapidly-varied free-surface flow in a rectangular channel is depicted in Figure 1. Reference is made to a Cartesian coordinate system, where x is horizontal in a streamwise direction; y is horizontal in the transverse direction; and z is vertically upward. The dynamic equation for free-surface flow, ignoring lateral flows, can be written as (Fenton and Zerihun, 2007)

$$\frac{\partial Q}{\partial t}+\beta\frac{\partial}{\partial x}\left(\frac{Q^2}{A}\right)+\frac{1}{\rho}\int_A\frac{\partial p}{\partial x}dA+\frac{fQ^2P_w}{8A^2}\left(1+\zeta_x^2\right)=0, \tag{1}$$

where f denotes the Darcy–Weisbach friction coefficient; Q is the discharge; A is the cross-sectional area of the flow; ρ is the density of the fluid; p is the pressure; β refers to the Boussinesq momentum coefficient; P_w is the wetted perimeter; ζ_x is the first derivative of the bed profile; and t is the time.

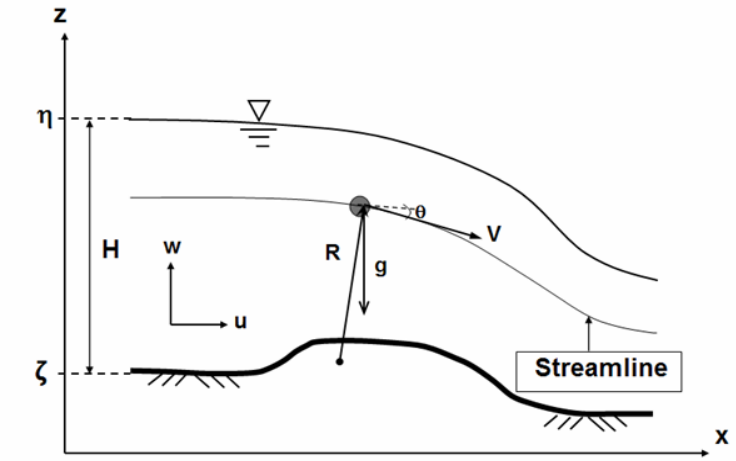

Figure 1. Definition sketch of a curved free-surface flow, showing the coordinates and variables of the numerical model. The tangential velocity of the fluid particle is denoted by V.

The Euler equation for the momentum balance in the z-direction is given by

$$\frac{1}{\rho}\frac{\partial p}{\partial z}=-g-a_z, \tag{2}$$

where g is acceleration due to gravity, and a_z is the vertical acceleration of the flow. Assuming that the rates of change of quantities over time are much slower than the apparent acceleration of a fluid particle following a curvilinear path (Fenton and Zerihun, 2007), the equation for the vertical acceleration may be written as

$$a_z=u\frac{\partial w}{\partial x}+w\frac{\partial w}{\partial z}=\kappa\frac{u^2}{\cos^3\theta}=u^2\xi, \tag{3}$$

where $\kappa(=1/R)$ is the curvature of the streamline; R is the radius of curvature; u is the horizontal velocity; w is the vertical velocity; and θ is the angle of inclination of the streamline with the horizontal axis. As in Zerihun (2008, 2016, 2017), a linear profile for the vertical distribution of the streamline geometry parameter, ξ, is assumed as follows:

$$\xi = \xi_b + (\xi_s - \xi_b)\lambda, \tag{4}$$

$$\lambda = \frac{z-\zeta}{\eta-\zeta}, \tag{5}$$

where η and ζ are the elevations of the free surface and channel bed, respectively; λ is a non-dimensional vertical height; and z is the vertical coordinate of a point in the flow field. The subscripts b and s refer to the magnitudes of the parameter at the channel bed and free surface, respectively. The variation of the horizontal velocity across the flow depth is also approximated by a linear relation (Zerihun, 2021) as follows:

$$u = \frac{q}{H}G(\omega,\lambda) = \frac{q}{H}\left(2\lambda(1-\omega)+\omega\right), \tag{6a}$$

$$\beta = \frac{1}{U^2}\int_0^1 u^2(\lambda)d\lambda = \frac{1}{3}\left(\omega^2 - 2\omega + 4\right), \tag{6b}$$

where $G(\omega,\lambda)$ determines the distribution shape of the horizontal component of the velocity; H is the flow depth; q is the discharge per unit width; U is the depth-averaged velocity; and ω is the velocity distribution parameter which can be determined from measurements.

Based on Leibnitz's rule, the integration of the continuity equation for a 2D flow can be written as

$$\int_z^\eta \frac{\partial u}{\partial x}dz + \int_z^\eta \frac{\partial w}{\partial z}dz = \frac{\partial}{\partial x}\left(\int_z^\eta u(z)dz\right) + u(z)z_x - u(\eta)\,\eta_x + w_s - w = 0, \tag{7}$$

where the subscript x denotes a partial differentiation with respect to the horizontal axis, and u_s and w_s are the free-surface velocity components in the horizontal and vertical directions, respectively.

By using Equation (6a), the first term on the right-hand side (RHS) of Equation (7) is integrated and then differentiated with respect to x. After applying the free-surface kinematic boundary condition, $w_s = \partial H/\partial t + (\partial\eta/\partial x)u_s$, the resulting expression is simplified to

$$\begin{aligned} w = {} & \frac{\partial H}{\partial t}\left(1-\omega(1-\lambda)-(1-\omega)\left(1-\lambda^2\right)\right) + \frac{q\eta_x}{H}(2-\omega) - \frac{2q\zeta_x}{H}\left((1-\omega)(1-\lambda)\right) \\ & - \frac{qH_x}{H}\left((1-\lambda)\omega\right) - \frac{2qH_x}{H}\left((1-\omega)\left(1-\lambda^2\right)\right). \end{aligned} \tag{8}$$

Substituting Equations (4) and (6a) into Equation (2) and then integrating the resulting expression from z to η results in the pressure distribution equation of Zerihun (2021), i.e.,

$$\frac{p}{\rho g} = H(1-\lambda) + \frac{Q^2}{gHB^2}\left(\zeta_{xx}\omega^2(1-\lambda) + \left(\frac{H_{xx}\omega^2}{2} + 2\zeta_{xx}\omega\,(1-\omega)\right)\left(1-\lambda^2\right)\right) + \frac{Q^2}{gHB^2}\left(\left(\zeta_{xx}(1-\omega)^2 + H_{xx}\omega\,(1-\omega)\right)\frac{4\left(1-\lambda^3\right)}{3} + H_{xx}(1-\omega)^2\left(1-\lambda^4\right)\right), \tag{9}$$

where B is the width of the channel, and ζ_{xx} is the second derivative of the bed profile. Unlike the pressure equation of Fenton and Zerihun (2007), the above equation includes a higher-order dynamic pressure correction that stems from terms accounting for the effects of the vertical curvatures of the streamline and a non-uniform horizontal velocity distribution. In the case of free-surface flow with negligible curvatures of streamline in a mild-slope channel, Equation (9) reduces to the well-known hydrostatic pressure equation, which corresponds to the shallow-water theory.

For a 2D flow on a vertical plane, the variation of the free-surface elevation in the transverse direction is normally insignificant; hence, the pressure is independent of *y*. By applying Leibnitz's rule, the integral of the pressure gradient term in Equation (1) becomes

$$\frac{1}{\rho}\int_A \frac{\partial p}{\partial x}\partial A = \frac{B}{\rho}\left(\frac{\partial}{\partial x}\int_\zeta^\eta p(z)dz + p(\zeta)\zeta_x - p(\eta)\eta_x\right). \tag{10}$$

Using Equation (9) in Equation (10), the first term on the RHS of Equation (10) is integrated and then differentiated with respect to *x*. After employing the dynamic boundary condition, $p(\eta) = 0$, at the free surface, the resulting expression is substituted into Equation (1) to give the following equation for flow in a rectangular channel (Zerihun, 2021):

$$\frac{\partial Q}{\partial t} + \left(\beta\frac{2}{H} + \frac{\sigma_1}{3}\zeta_{xx} + \frac{2\sigma_2}{15}H_{xx}\right)\frac{Q}{B}\frac{\partial Q}{\partial x} + \frac{\sigma_2}{15}\frac{Q^2}{B}H_{xxx} + \frac{\sigma_1}{6}\frac{Q^2}{A}\zeta_x H_{xx} + \left(gA - \beta\frac{Q^2B}{A^2}\right)H_x + \frac{Q^2}{A}\left(\frac{\sigma_1}{6}\zeta_{xxx}H + \frac{\sigma_3}{3}\zeta_{xx}\zeta_x\right) + gA\zeta_x + \frac{fQ^2P_w}{8A^2}\left(1+\zeta_x^2\right) = 0, \tag{11a}$$

$$\sigma_1 = \omega^2 - 4\omega + 6, \tag{11b}$$

$$\sigma_2 = 2\omega^2 - 9\omega + 12, \tag{11c}$$

$$\sigma_3 = \omega^2 - 2\omega + 4, \tag{11d}$$

where ζ_{xxx} is the third derivative of the bed profile. The non-linear coefficients associated with the spatial derivative terms of the above equation take into account the effect of a non-uniform horizontal velocity distribution in addition to the effect of the vertical acceleration of the flow. If the scope of the study is limited to steady-flow conditions, then by definition $\partial A/\partial t = B\partial H/\partial t = \partial Q/\partial x = 0$. Using this fact, Equation (11a) simplifies to

$$\frac{\sigma_2}{15}\frac{Q^2}{B}H_{xxx} + \frac{\sigma_1}{6}\frac{Q^2}{A}\zeta_x H_{xx} + \left(gA - \beta\frac{Q^2B}{A^2}\right)H_x + \frac{Q^2}{A}\left(\frac{\sigma_1}{6}\zeta_{xxx}H + \frac{\sigma_3}{3}\zeta_{xx}\zeta_x\right) + gA\zeta_x + \frac{fQ^2P_w}{8A^2}\left(1+\zeta_x^2\right) = 0. \tag{12}$$

Equation (12) is a higher-order depth-averaged equation for steady, 2D free-surface flow problems, where the effects of the non-hydrostatic pressure and non-uniform velocity distributions are significant. The flow resistance term appearing in this equation is estimated by using the Darcy–Weisbach equation with an explicit form of the Colebrook–White formula (Zigrang and Sylvester, 1982) for the friction factor. In the case of free-surface flows with a uniform velocity and a hydrostatic pressure distribution in a constant slope channel, Equation (11a) reduces to the Saint-Venant equation. In contrast to the Bose and Dey (2007) equations, the present model is not restricted to weakly-curved flow situations.

In this study, Equations (6a), (8), (9), and (12) will be employed to obtain detailed descriptions of the local and global flow characteristics of free overfall in rectangular channels with smooth and rough beds. In these equations, the unknowns to be solved numerically using a finite-difference scheme are the velocity and pressure distributions and the depth of flow. The numerical solutions of the equations will be compared with the measurements in order to determine the validity of the proposed model for curved-flow problems with dual free surfaces.

2.1.1 Boundary conditions

The numerical solution of the flow problem requires three boundary conditions for the upper free-surface profile and two boundary conditions for the lower nappe profile to be specified at the appropriate flow sections. The inflow section of the computational domain is located in a region where the effect of the vertical curvatures of the streamline is insignificant. Hence, the free-surface slope, S_H, at this section can be computed by using a gradually-varied flow equation,

$$S_H = \eta_x = \frac{S_0 - S_f}{1 - \beta F^2} + \zeta_x, \tag{13a}$$

$$S_f = \frac{fq^2\left(1+\zeta_x^2\right)}{8gR_h H^2}, \tag{13b}$$

where F is the Froude number; S_f is the friction slope; R_h is the hydraulic radius; and S_0 is the bed slope.

At the brink section, two internal boundary conditions – an atmospheric bed pressure and a constant bed elevation – are imposed. Besides, the elevation of the lower nappe at outflow section is specified and remained unchanged during the computations. For the purpose of simulating the free-surface and pressure profiles, the computational domain is discretized into equal size steps in x, as shown in Figure 2.

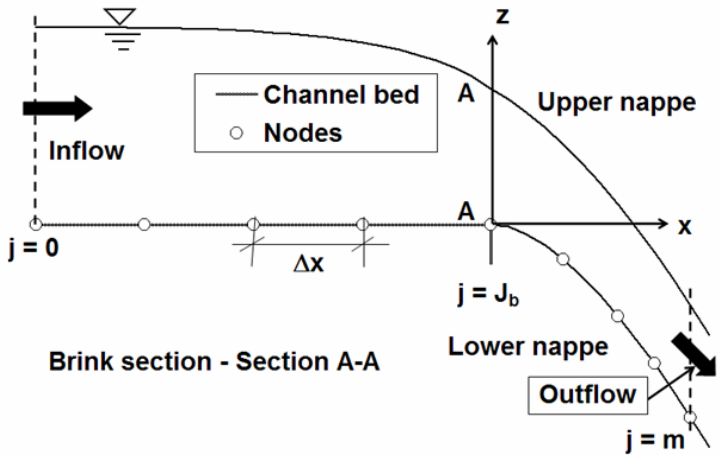

Figure 2. Definition sketch and computational domain for the free-overfall problem.

2.2 Numerical model

Because of its non-linear nature, a closed-form solution cannot be obtained for Equation (12). This equation includes a third-order spatial derivative term; hence, it requires a third- or higher-order accurate numerical scheme for its solution (Abbott et al., 1978). For the purpose of discretization, Equation (12) can be rewritten in the following form:

$$H_{xxx,j} + \xi_{0,j} H_{xx,j} + \xi_{1,j} H_{x,j} + \xi_{2,j} = 0, \tag{14}$$

where $\xi_{0,j}$, $\xi_{1,j}$ and $\xi_{2,j}$ are the non-linear coefficients associated with the equation. The first, second, and third spatial derivative terms, which appear in the above equation, are discretized by using the finite-difference approximations (Bickley, 1941). After simplifying and combining similar terms together, the resulting expression becomes

$$\begin{aligned} &6\xi_{2,j}(\Delta x)^3 + H_{j-2}\left(-6 + \xi_{1,j}(\Delta x)^2\right) + H_{j-1}\left(18 + 6\xi_{0,j}\Delta x - 6\xi_{1,j}(\Delta x)^2\right) \\ &+ H_j\left(-18 - 12\xi_{0,j}\Delta x + 3\xi_{1,j}(\Delta x)^2\right) + H_{j+1}\left(6 + 6\xi_{0,j}\Delta x + 2\xi_{1,j}(\Delta x)^2\right) = 0, \end{aligned} \tag{15}$$

where Δx is the step size. Since the flow depth at the inflow section ($j = 0$) is known, the depth at the imaginary node ($j = -1$) can be determined from the estimated free-surface slope at $j = 0$. Using the discretized form of Equation (13a) at this section and the expanded form of Equation (15) at $j = 0$, the following implicit finite-difference equation is obtained for predicting the depth at $j = -1$:

$$\begin{aligned} &H_{-1}\left(-18 + 6\xi_{0,0}\Delta x\right) - H_0\left(12\xi_{0,0}\Delta x\right) + H_1\left(18 + 6\xi_{0,0}\Delta x\right) \\ &+ 6S_H\left(-6\Delta x + \xi_{1,0}(\Delta x)^3\right) + 6\xi_{2,0}(\Delta x)^3 = 0. \end{aligned} \tag{16}$$

To simulate the fixed bed and the free jet portion of the flow together, the elevations of the lower nappe and the upper free-surface profile of the entire flow region and the bed pressure along the fixed bed channel are considered as unknowns. For the free jet portion, the pressure at the underside of the nappe is atmospheric. Using this known condition, the following discretized equation for the elevation of the lower nappe of the jet, ζ, is obtained from the pressure equation:

$$\left(\zeta_{j-1} - 2\zeta_j + \zeta_{j+1}\right) + \frac{3gH_j^2(\Delta x)^2}{q^2\left(\omega^2 - 2\omega + 4\right)} + \left(\frac{\omega^2 - 4\omega + 6}{2\left(\omega^2 - 2\omega + 4\right)}\right)\left(H_{j-1} - 2H_j + H_{j+1}\right) = 0\,. \tag{17}$$

For the solution of the lower nappe profile, the elevation of the nappe at the outflow section ($j = m$) is specified as a boundary condition. At the junction between the free jet and the fixed bed ($j = J_b$), the elevation of this nappe is also known. As noted by Hager (1983), the inclination of the free-surface profile of the lower nappe at the brink section varies with the Froude number of the incoming flow. This implies that the jet does not tangentially leave the brink section. Using the specified internal boundary condition (atmospheric bed pressure), the discretized equation for the curvature of the upper nappe profile is obtained from the pressure equation as follows:

$$H_{j-1} - 2H_j + H_{j+1} = -\left(\frac{6gH_j^2(\Delta x)^2}{q^2\left(\omega^2 - 4\omega + 6\right)}\right) - 2\left(\frac{\omega^2 - 2\omega + 4}{\omega^2 - 4\omega + 6}\right)\left(\zeta_{j-1} - 2\zeta_j + \zeta_{j+1}\right); \quad j = J_b. \tag{18}$$

The use of Equation (15) at the outflow section introduces an unknown nodal value external to the solution domain. Hence, discretizing the derivatives using the backward finite-difference equations eliminates this problem. Following the same procedure of discretization, the finite-difference equivalent equation for this node becomes

$$\begin{aligned} &H_{j-4}\left(36+22\xi_{0,j}\Delta x+6\xi_{1,j}(\Delta x)^2\right)+H_{j-3}\left(-168-112\xi_{0,j}\Delta x-32\xi_{1,j}(\Delta x)^2\right)\\ &+H_{j-2}\left(288+228\xi_{0,j}\Delta x+72\xi_{1,j}(\Delta x)^2\right)+H_{j-1}\left(-216-208\xi_{0,j}\Delta x-96\xi_{1,j}(\Delta x)^2\right)\\ &+H_{j}\left(60+70\xi_{0,j}\Delta x+50\xi_{1,j}(\Delta x)^2\right)+24(\Delta x)^3\xi_{2,j}=0. \end{aligned} \tag{19}$$

The above implicit set of non-linear algebraic equations is solved by the Newton–Raphson iterative method with a numerical Jacobian matrix which proceeds from the assumed initial free-surface positions. First, the initial lower nappe profile is obtained by linearly interpolating the channel bed elevation at the brink section and the boundary value at the outflow section. The Bernoulli and continuity equations are then employed to obtain the initial free-surface profile for the upstream portion of the flow and the upper nappe. Since the curvature of the fixed bed is known, Equations (15), (16), (18), and (19) with the specified inflow boundary conditions are solved numerically to simulate the upper free-surface profile. To predict the lower nappe profile, Equation (17), together with the specified two boundary conditions, is solved using a similar technique. The convergence of the numerical solutions is assessed based on the relative change in solution criterion with a convergence tolerance of 10^{-6}.

For the numerical solution of the pressure equation, a similar finite-difference formula is inserted into Equation (9) to discretize its derivative term. The discretized equation is employed to compute the pressure profiles using the predicted flow depths.

3. APPLICATION TO CURVILINEAR FLOWS

This section examines the application of the proposed model to rectangular free-overfall problems with super- and sub-critical approach flows by comparing the numerical results with the experimental data available. For all the test cases considered, the size of the computational steps was designed to vary between 8 and 20% of the depth of flow at the inflow section. Consequently, all computational results presented here were free of any numerical errors arising from the effect of spatial discretization.

As described before, a pre-determined velocity distribution parameter, ω, is necessary in order to accurately simulate the local flow characteristics of the free-overfall problems. In this study, the value of this parameter was estimated using the experimental data of Rajaratnam and Muralidhar (1968). For ω = 0.97, the computed non-dimensional horizontal velocity profile, u/U, showed a fairly good correlation with the measured data with a mean relative error of 3.8%, as shown in Figure 3a. Likewise, Figure 3b compares the predicted non-dimensional vertical velocity profiles, w/U_c (U_c is the critical velocity), with the experimental data. Although the accuracy of the results of the model was slightly deteriorated at the brink section, the predicted profiles correlated reasonably well with the measured data. Overall, the profiles of the horizontal and vertical velocities across the flow depth were satisfactorily simulated by the proposed velocity distribution equations. Based on the calibration result, the ω values of 0.97 and 1.15 were used for the flow regions upstream and downstream of the brink section, respectively, to simulate the 2D curvilinear flows.

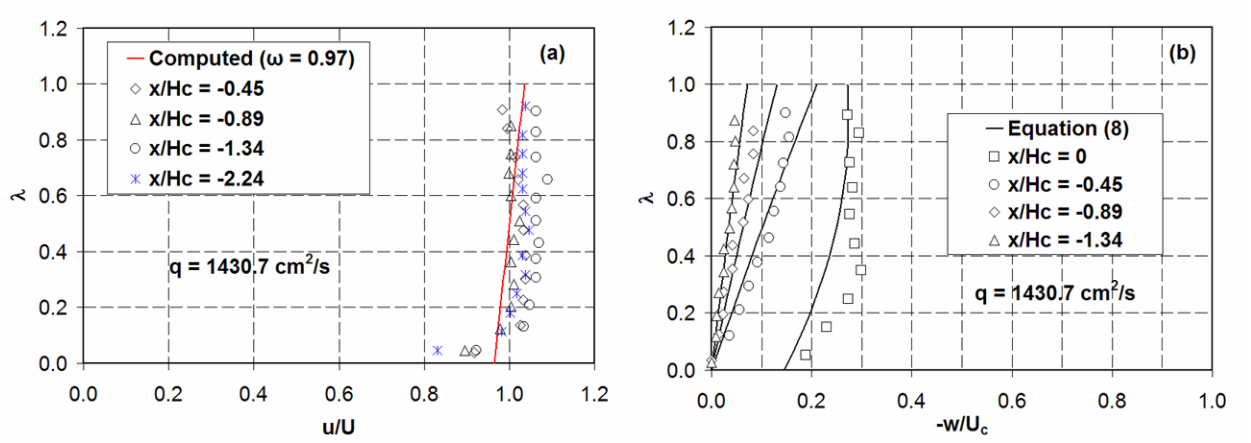

Figure 3. Velocity field of the rectangular free overfall with a subcritical approach flow: (a) horizontal velocity distribution; and (b) vertical velocity distribution.

3.1 Model results for a smooth bed channel

3.1.1 Supercritical approach flow

Figure 4 shows the comparison of the predicted upper free-surface and lower nappe profiles with the experimental data of Rajaratnam and Muralidhar (1968) and Marchi (1993). In this figure, the dimensionless free-surface elevation, η/H_c (H_c is the critical depth), is shown versus the normalized distance from the brink, x/H_c. Upstream of the free overfall, the agreement between the results of the model and the experimental data was remarkable, with a maximum relative error of less than 1%. The result of the simulation for the lower nappe profile also agreed well with Marchi's (1993) measured data, as shown in Figure 4a. Since the control section for the supercritical flow is at the upstream end, the significance of the brink depth is completely different from the case of a subcritical approach flow, and its value depends on the Froude number of the incoming flow and bed slope (Rajaratnam and Muralidhar, 1968). In this case, the discharge can be estimated from the measurement of brink depth and knowledge of bed slope and channel roughness.

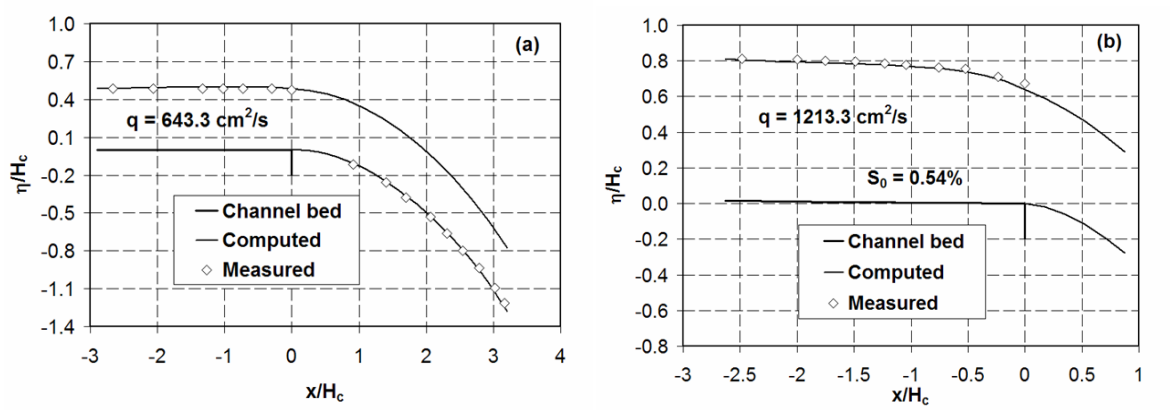

Figure 4. Comparison of predicted and measured free-surface profiles for a rectangular free overfall: (a) horizontal channel; and (b) mild-slope channel.

3.1.2 Subcritical approach flow

The computed free-surface profiles for a subcritical approach flow are compared with the experimental data in Figures 5 and 6. Upstream of the brink section, the results of the model were in good agreement with the experimental data for all flow rates. Furthermore, the result of the model

for the lower nappe profile of the jet corresponded well with the measured data (see Figure 5). This numerical experiment indicates that the present model is capable of accurately simulating the free-overfall problem with a subcritical inflow condition irrespective of the degree of the vertical curvatures of the streamline. For a subcritical inflow condition, the brink depth, H_b, is an important parameter for estimating the flow rate. This depth is influenced by both the slope and bed roughness, with roughness having a greater effect at steeper slopes (Davis et al., 1998). As can be seen from Figure 7, the brink depth was satisfactorily predicted, with a mean relative error of 2.5%.

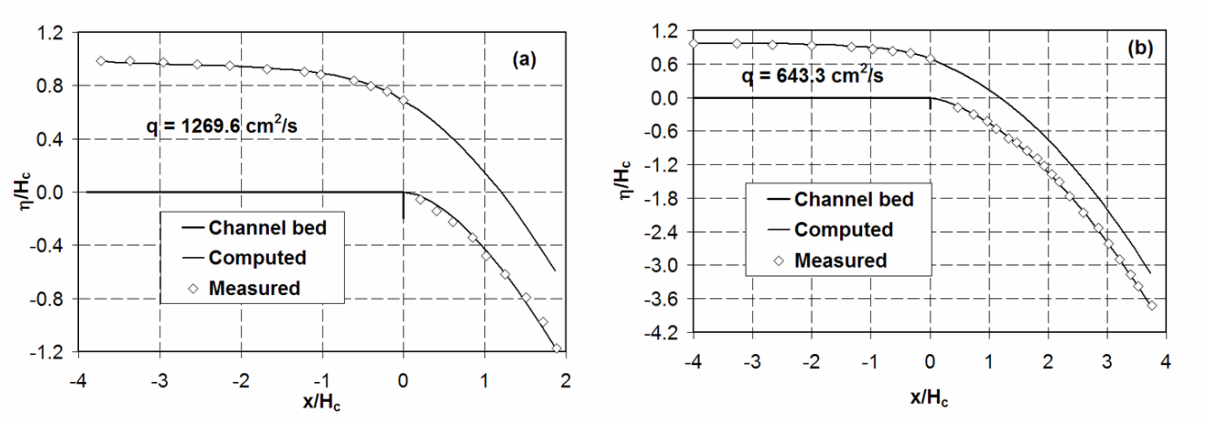

Figure 5. Free-surface profiles for free overfall with a subcritical inflow condition. The numerical results are compared with the experimental data of Marchi (1993).

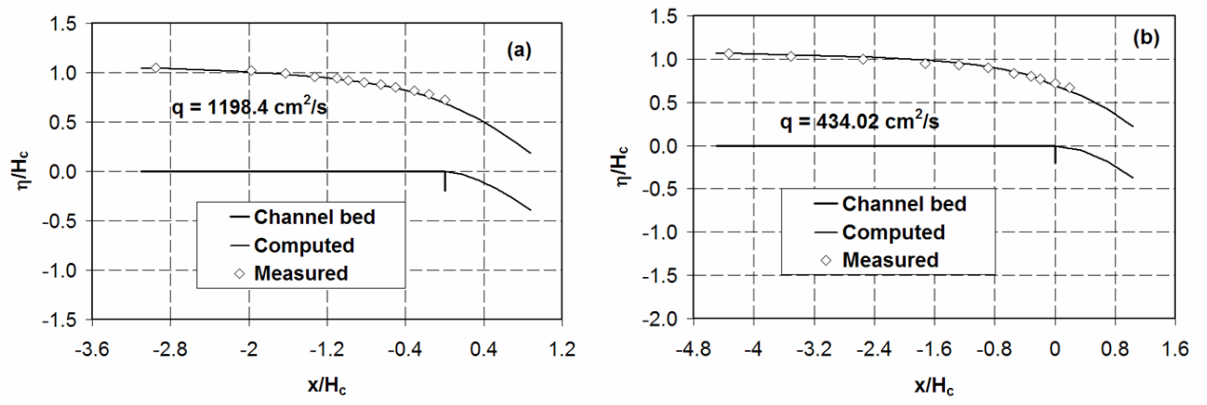

Figure 6. Free-surface profiles for free overfall with a subcritical inflow condition. The experimental data of Rajaratnam and Muralidhar (1968) and Rouse (1933) are used to validate the numerical results in (a) and (b), respectively.

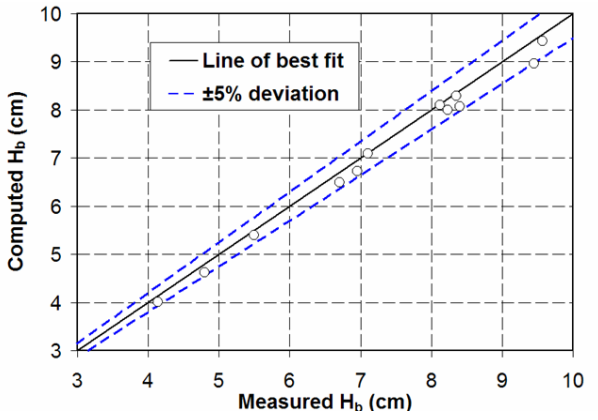

Figure 7. Comparison of the computed brink depth with the experimental data of Rouse (1932, 1933), Rajaratnam and Muralidhar (1968), and Rajaratnam et al. (1976).

3.1.3 Pressure distributions

Figure 8 shows the bed-pressure profile upstream of the brink section. In this figure, the non-dimensional bed pressure at any section, $p_b / \gamma H_c$ (p_b is the bed pressure, γ is the unit weight of the fluid), is shown versus the normalized distance from the brink, x / H_c. As can be seen, the predicted result compared well with the experimental data. The maximum relative error in the numerical result of the model was about 3%. As expected, the result demonstrates the strong dependence of the bed-pressure distribution on the dynamic effects of the flow due to streamline curvilinearity.

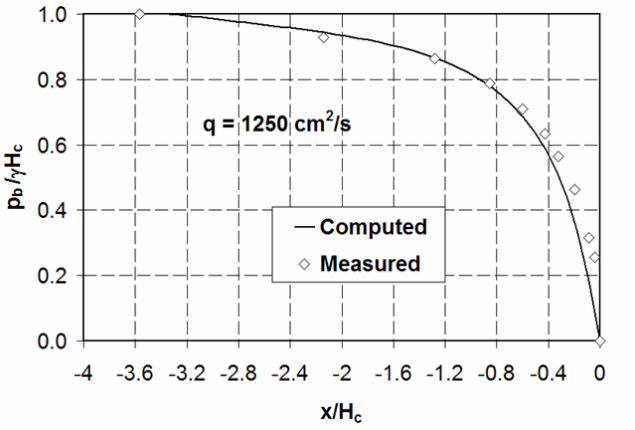

Figure 8. Bed-pressure profile for free overfall with a subcritical inflow condition. The numerical result is compared with the experimental data of Rouse (1932).

Figure 9 shows the computed and measured non-dimensional pressure profiles, p / p_0 (p is the pressure at a point in the flow field, p_0 is the hydrostatic pressure at the bed), versus the dimensionless vertical height above the bed, λ, at various sections upstream of the overfall. It can be seen from this figure that the result of the model for the pressure distribution at the brink section was satisfactory and followed a similar pattern to the observed values. Similar model performance results can be seen at vertical sections $x / H_c = -0.56$, $x / H_c = -1.11$, and $x / H_c = -1.67$ to the left of the brink section, where the vertical curvatures of the streamline are moderate. As the upstream distance from the brink section increases, the influence of the curvature of the streamline becomes insignificant. Consequently, the pressure distribution gradually approaches hydrostatic (see Figure 9). The above validation results for super- and sub-critical approach flows showed that the present model accurately simulated the transition between hydrostatic and non-hydrostatic flow regimes.

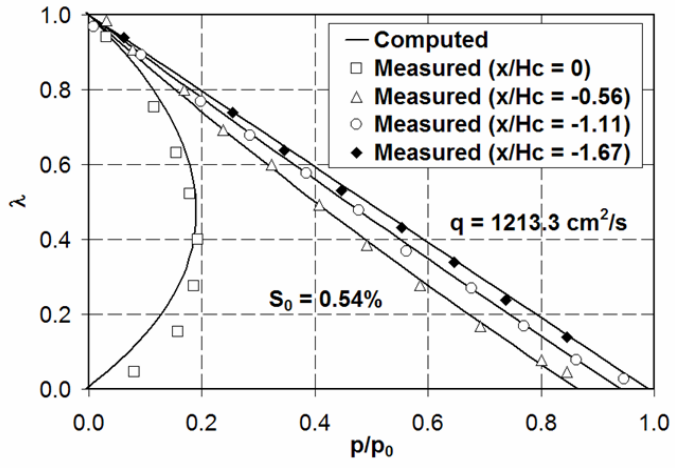

Figure 9. Comparison of the computed results for the vertical profile of the pressure with the experimental data of Rajaratnam and Muralidhar (1968).

3.2 Model results for a rough bed channel

Rajaratnam et al. (1976) conducted a number of experiments for free overfall in a rectangular channel with different values of discharge and bed roughness. The experiment with a flow of 1454.9 cm^2/s and bed roughness simulated using a 3.4 mm diameter wire screen (a mesh size of 9.6 mm) was chosen to validate the results of the model. The Darcy–Weisbach friction coefficient for the rough bed was predicted based on the suggested equivalent roughness height of 11.9 mm and was taken as constant throughout the computational domain of the fixed bed channel.

For the subcritical approach flow, the simulated free-surface profile is compared with the experimental data in Figure 10. The model accurately predicted the free-surface elevations near the brink section where the streamlines have steep slope and pronounced curvature. Upstream of this section, the numerical solution of the model agreed well with the experimental result. In general, the overall qualities of the result of the model were satisfactory.

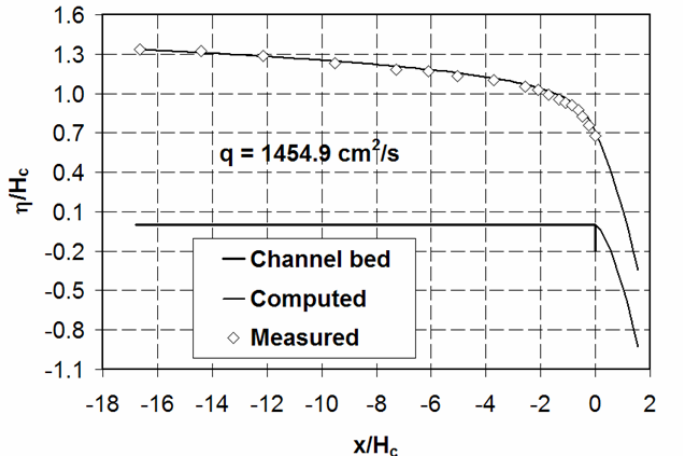

Figure 10. Free-surface profile for a rectangular free overfall in a rough bed channel.

4. DISCUSSION

Previous studies (e.g., Matthew, 1995; Khan, 1999; Di Nucci and Russo Spena, 2018; Zerihun, 2004, 2021) demonstrated that the Boussinesq-type equations can provide reasonably accurate solutions to the problems of free-surface flow with strong curvilinear effects. Depending on the methods of the derivation, these equations incorporate different degrees of approximation for the effects of the vertical curvatures of the streamline. The numerical solutions of such types of non-linear equations generally require the specification of appropriate boundary conditions with a mathematical treatment of the discontinuity problem of the bottom profile. The aim of this treatment is to smooth out the discontinuity, so that physically unrealistic simulation results such as high pressure spikes at a break in bottom slope can be easily eliminated. Without applying short transition curves at the corners, Castro-Orgaz and Hager (2019, pp. 456-457) numerically solved the weir flow problem. They obtained results that look like the bed-pressure distribution of a flow separated from the weir bottom (see Zerihun, 2020). The accuracy of these results, however, suffered from the assigned arbitrary values of the bottom geometry parameters at the corner nodes.

The overall validation results of the present numerical model highlighted the importance of the above numerical technique for accurately modeling the problem of free overfall in rectangular channels with smooth and rough beds. Improper implementation of the numerical procedures may result in deceptive numerical results, especially for the local flow characteristics of the highly curvilinear flow problem (also see Montes, 1994; Di Nucci and Russo Spena, 2011). As noted by Zerihun (2004), the order of approximation for the effects of the streamline curvature has only a marginal impact on the predictions of the free-surface and bed-pressure profiles. In contrast, the numerical results of the velocity and pressure distributions are very sensitive to the level of

approximation which has been maintained for such effects. This investigation also reveals that the 2D structure of the curvilinear flow field can be adequately described by considering not only the effect of the free-surface curvature but also the effect of the bottom curvature. Such a modeling approach does not make the practical applications of the Boussinesq-type equations mathematically cumbersome.

5. CONCLUSIONS

A numerical investigation was carried out to assess the suitability of a depth-averaged Boussinesq-type model for complex open-channel flow problems with dual free surfaces such as rectangular free overfalls in smooth and rough bed channels. In comparison with earlier works, the proposed model includes a higher-order dynamic pressure correction that arises not only from the applied non-uniform velocity distribution but also from terms accounting for the effects of the vertical curvatures of the streamline. A finite-difference method was employed to discretize the model equations. As direct solutions for the free-surface profile cannot be obtained owing to an implicit form of the discretized equations, the Newton–Raphson iterative method with a numerical Jacobian matrix was used to solve the resulting non-linear algebraic equations. The predictions of the model were then compared with the experimental data for free overfalls with super- and sub-critical approach flows.

For all the test cases, the results of the validation showed good correlation between the numerical results and the experimental data for free-surface and bed-pressure profiles and distributions of velocity and pressure, thereby demonstrating the validity of the proposed model for a non-hydrostatic flow with dual free surfaces. The satisfactory performance of the present model in these test cases may be attributed to the higher-order dynamic pressure correction implicitly incorporated in the model. By treating the fixed bed and the free jet portion of the flow as a single curved-flow problem, the numerical scheme accounted for the effects of the curvature of the lower nappe throughout the computational domain and overcame the drawbacks of the existing methods which consider only the fixed bed part of the flow. The results of this study highlighted the reliability of the current computational scheme for developing a discharge rating curve (brink-depth-discharge relationships) for a laterally-guided free overfall with a subcritical approach flow.

REFERENCES

Abbott, M. B., Petersen, H. M. and Skovgaard, O. (1978) On the numerical modeling of short waves in shallow water, J. Hydraul. Res., 16(3), 173–204.

Bickley, W. G. (1941) Formulae for numerical differentiation, Math. Gaz., 25(263), 19–27, doi: 10.2307/3606475.

Bos, M. G. (1989) Discharge Measurement Structures, 3rd rev. ed.; International Institute for Land Reclamation and Improvement: Wageningen, The Netherlands.

Bose, S. and Dey, S. (2007) Curvilinear flow profiles based on Reynolds-averaging, J. Hydraul. Eng., 133(9), 1074–1079.

Castro-Orgaz, O. and Hager, W. H. (2011) Vorticity equation for the streamline and the velocity profile, J. Hydraul. Res., 49(6), 775–783.

Castro-Orgaz, O. and Hager, W. H. (2019) Shallow Water Hydraulics, Springer Nature Switzerland AG, Cham, Switzerland.

Davis, A. C., Ellett, B. G. and Jacob, R. P. (1998) Flow measurement in sloping channels with rectangular free overfall, J. Hydraul. Eng., 124(7), 760–763.

Dey, S. (2002) Free overfall in open channels: State-of-the-art review, Flow Meas. Instrum., 13(5), 247–264.

Di Nucci, C. and Russo Spena, A. (2011) A discussion to “Moment of momentum equation for curvilinear free-surface flow”, J. Hydraul. Res., 49(3), 415–419.

Di Nucci, C. and Russo Spena, A. (2018) On the steady two-dimensional open-channel flow, J. Interdiscip. Math., 21(3), 579–594.

Fenton, J. D. and Zerihun, Y. T. (2007) A Boussinesq approximation for open-channel flow, In: Proceedings of the 32nd Congress, IAHR, Venice, Italy, 2–6 July.

Guo,Y. (2005), Numerical modeling of free overfall, J. Hydraul. Eng., 131(2), 134–138.

Guo, Y., Zhang, L., Shen, Y. and Zhang, J. (2008) Modeling study of free overfall in a rectangular channel with strip roughness, J. Hydraul. Eng., 134(5), 664–667.

Hager, W. H. (1983) Hydraulics of plane free overfall, J. Hydraul. Eng., 109(12), 1683–1697.

Jaeger, C. (1948) Hauteur d’eau à l’extrémité d’un long déversoir (Flow depth at the extremity of a long weir), La Houille Blanche, 3(6), 518–523 [in French].

Khan, A. A. (1999) Modeling rectangular overfalls using Boussinesq equations, Proc. Instn. Civ. Eng., Water, Maritime and Energy, London, England, 136(2), 77–80.

Le Méhauté, B (1969) An Introduction to Hydrodynamics and Water Waves – Volume 1: Fundamentals, ESSA Technical Report, ERL 118-POL 3-1, Miami, FL, USA.

Matthew, G. D. (1995) A discussion to "A potential flow solution for the free overfall", Proc. Instn. Civ. Eng., Water, Maritime and Energy, London, England, 112(1), 81–85.

Marchi, E. (1993) On the free overfall, J. Hydraul. Res., 31(6), 777–790.

Montes, J. S. (1992) A potential flow solution for the free overfall, Proc. Instn. Civ. Eng., Water, Maritime and Energy, London, England, 96(4), 259–266.

Montes, J. S. (1994) A discussion to "On the free overfall", J. Hydraul. Res., 32(5), 792–794.

Nakagawa, H. (1969) Flow Behaviors near the Brink of Free Overfall, Bulletin of the Disaster Prevention Research Institute, Kyoto University, 18(4), 66–76. Retrieved from https://hdl.handle.net/2433/124760.

Pal, M. and Goel, A. (2006) Prediction of the end-depth ratio and discharge in semicircular- and circular-shaped channels using support vector machines. Flow Meas. Instrum., 17(1), 49–57.

Pal, M. and Goel, A. (2007) Estimation of discharge and end depth in trapezoidal channel by support vector machines, Water Resour. Manag. 21(10), 1763–1780.

Raikar, R. V., Nagesh Kumar, D. and Dey, S. (2004) End-depth computation in inverted semicircular channels using ANNs, Flow Meas. Instrum., 15(5-6), 285–293.

Rajaratnam, N. and Muralidhar, D. (1968) Characteristics of the rectangular free overfall, J. Hydraul. Res., 6(3), 233–258.

Rajaratnam, N., Muralidhar, D. and Beltaos, S. (1976) Roughness effects on rectangular free overfall, J. Hydraul. Div., 102(HY5), 599–614.

Ramamurthy, A. S., Qu, J. and Vo, D. (2005) Volume of fluid model for an open-channel flow problem, Can. J. Civ. Eng., 32(5), 996–1001.

Ramamurthy, A. S., Qu, J. and Vo, D. (2006) Volume of fluid model for simulation of a free overfall in trapezoidal channels, J. Irrig. Drain. Eng., 132(1), 425–428.

Rouse, H. (1932) The Distribution of Hydraulic Energy in Weir Flow in Relation to Spillway Design, Master's Thesis, Massachusetts Institute of Technology, Boston, MA, USA.

Rouse, H. (1933) Verteilung der Hydraulischen Energie bei einem Lotrechten Absturz (Distribution of Hydraulic Energy at a Vertical Drop), Ph.D. Thesis, TU Karlsruhe, Karlsruhe, Germany [in German].

Sharifi, S., Sterling, M. and Knight, D. W. (2010) Prediction of end-depth ratio in open channels using genetic programming, J. Hydroinform., 13(1), 36–48.

Zerihun, Y. T. (2004) A One-Dimensional Boussinesq-Type Momentum Model for Steady Rapidly-Varied Open-Channel Flows, Ph.D. Thesis, Department of Civil and Environmental Engineering, The University of Melbourne, Australia.

Zerihun, Y. T. (2008) Development and validation of a one-dimensional non-hydrostatic open-channel flow model. In: Proceedings of the 31st Hydrology and Water Resources Symposium, and the 4th International Conference on Water Resources and Environment Research, Adelaide, Australia, 15–17 April, 2485–2495.

Zerihun, Y. T. (2016) Modeling free-surface flow with curvilinear streamlines by a non-hydrostatic model, J. Hydrol. Hydromech., 64(3), 281–288.

Zerihun, Y. T. (2017) A numerical study of non-hydrostatic shallow flows in open channels, Arch. Hydro-Eng. Environ. Mech., 64(1), 17–35.

Zerihun, Y. T. (2020) Free flow and discharge characteristics of trapezoidal-shaped weirs, Fluids, 5(4), doi: 10.3390/fluids5040238.

Zerihun, Y. T. (2021) Non-hydrostatic transitional open-channel flows from a supercritical to a subcritical state, Slovak J. Civ. Eng., 29(2), 39–48.

Zigrang, D. J. and Sylvester, N. D. (1982) Explicit approximations to the solution of Colebrook's friction factor equation, AIChE J., 28(3), 514–515.